Journal of Applied Electrochemistry
https://doi.org/10.1007/s10800-024-02144-6

RESEARCH ARTICLE

The corrosion behavior of electroless Ni–P coatings in concentrated KOH electrolyte

A. He[1] · H. Hu[1] · D. Aasen[2] · D. G. Ivey[1]

Received: 10 January 2024 / Accepted: 18 May 2024

Abstract

Ni–P has been widely used as a protective coating for many substrates. The corrosion resistance of Ni–P in neutral solutions such as NaCl, or acidic electrolytes such as HCl and H_2SO_4, has been extensively studied. However, the corrosion behavior of Ni–P coatings in caustic media, such as KOH, has received much less attention. Typically, corrosion behavior is studied through the use of electrochemical methods with corrosion rates determined from corrosion currents and potentials measured from Tafel curves. In this work, the corrosion rates of Ni–P coatings, with P concentrations varying from 2 to 11 wt%, in highly alkaline KOH (11 M) are obtained directly through electron microscopy measurements of cross sections and subsequent correlation with electrochemical data. Phosphorus concentration affects the corrosion rate; corrosion rate increases with increasing P content, peaks out at about 6–8 wt% P, and then decreases with any further increase in P content. This behavior is correlated to internal stress levels developed in the coatings.

✉ D. G. Ivey
divey@ualberta.ca

[1] Department of Chemical and Materials Engineering, University of Alberta, Edmonton, AB T6G 1H9, Canada

[2] Zinc8 Energy Solutions Inc, Vancouver, BC V6P 6T3, Canada

Published online: 07 June 2024

Graphical abstract

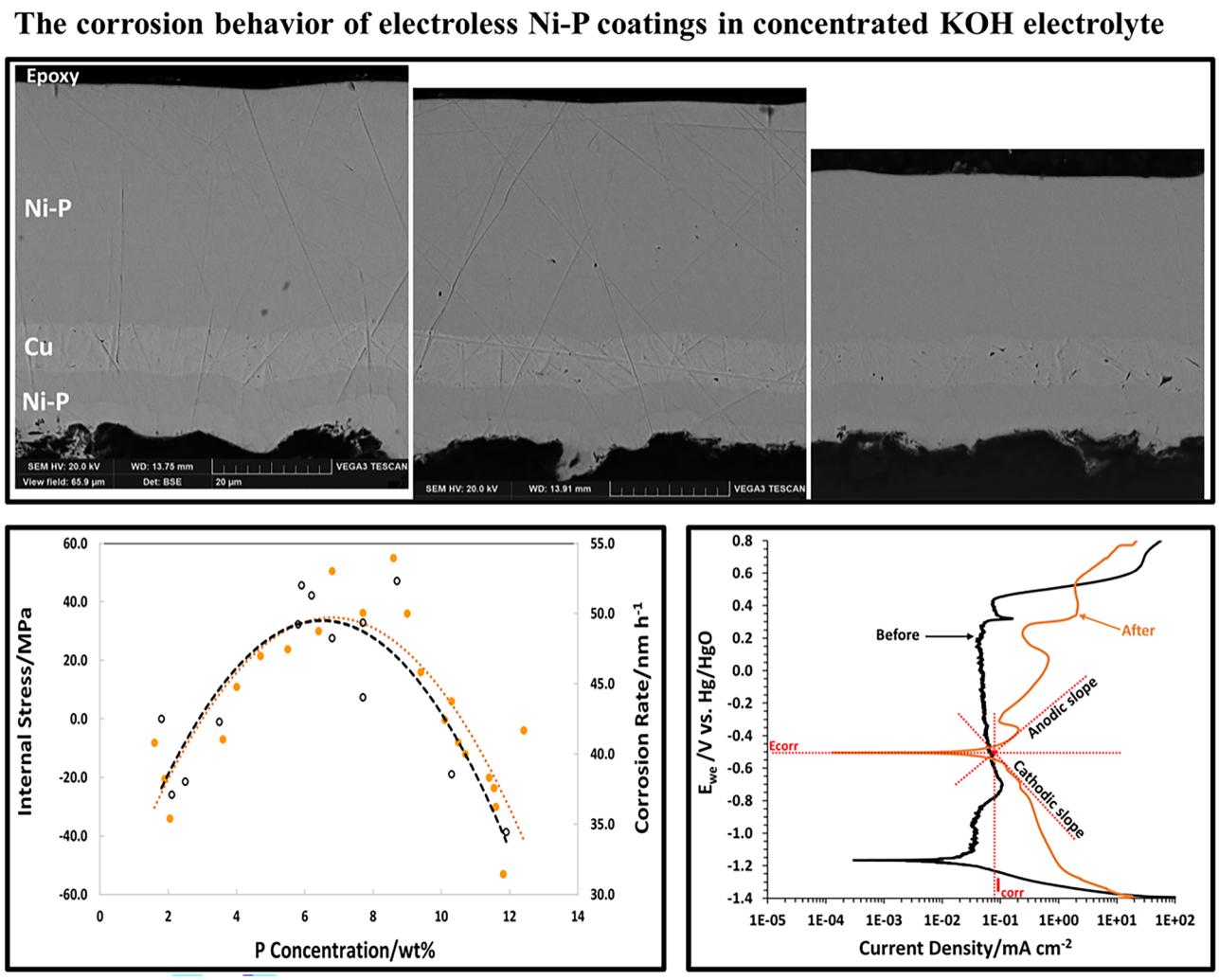

Keywords Ni–P coating · P content · Corrosion rate · Alkaline electrolytes

1 Introduction

Ni–P coatings have been widely used to protect various kinds of surfaces, both metallic and non-metallic, due to their good wear resistance, high hardness, solderability, and corrosion resistance. Ni–P represents over 95% of industrial electroless coatings [1–5]. In the last few decades, the mechanical properties of the coatings, such as hardness and wear resistance, have been extensively studied for as-deposited films and after heat treatment. Researchers are now focusing on adding third, or even fourth elements, or nanoparticles to further improve the mechanical properties of Ni–P coatings [2]. There is a general consensus in the available literature concerning the corrosion resistance of Ni–P coatings in neutral (e.g., 3 or 3.5 wt% NaCl) or acidic solutions (e.g., HCl or H_2SO_4) that a higher P content provides better corrosion resistance [4–11].

In contrast to corrosion resistance studies in neutral or acidic electrolytes, reports regarding the corrosion behavior of Ni–P in alkaline solutions are mixed. For example, Lo et al. [12] reported that the corrosion resistance is enhanced with increasing P content in 40 wt% NaOH, while Kang et al. [13] pointed out that an amorphous Ni–P coating (with a high P content) is not suitable for a 6 M KOH environment. Zeller et al. [14] reported that in 50 wt% NaOH electrolyte, Ni–P coatings with 5.0 wt% P had the lowest corrosion rate while coatings with 10.5 wt% P had the highest corrosion rate. Ni–P coatings with 2.0 wt% P had corrosion rates between the two extreme values. A common feature of

the work by Ho et al. [12] and Kang et al. [13] was that the electrolytes were degassed either with N_2 [12] or Ar [13] to remove dissolved oxygen before electrochemical testing. In Zeller et al.'s work, the electrolyte was open to the atmosphere to maintain an O_2-rich condition [14].

Besides the aforementioned inconsistent corrosion resistance behavior, it is of interest to further study the corrosion behavior of Ni–P in alkaline environments, with a wide range of P contents, since Ni–P alloys can be used as catalysts for the hydrogen evolution reaction (HER) for gaseous hydrogen generation through water electrolysis [15, 16] and for the oxygen evolution reaction (OER) during battery charging [17–19]. In both cases, a highly alkaline environment can be encountered. One example is the electrolytes for Zn-air type batteries which are highly alkaline with concentrations as high as 45% KOH (11 M KOH) [17–19]. It is beneficial to evaluate the corrosion behavior of Ni–P under alkaline conditions, since corrosion can affect electrode lifetime and operation cost.

This work aims to investigate the corrosion behavior of Ni–P coatings in an extremely caustic alkaline electrolyte (11 M KOH) over a wide range of P content. Conventional electrochemical testing techniques and direct measurements of coating thickness and morphology changes are employed and compared. It is shown that direct measurements should be utilized whenever possible to obtain more reliable corrosion rate data.

2 Experimental methods

2.1 Sample selection and preparation

Ni–P coatings can be electrolessly deposited from either alkaline electrolyte [20] or acidic electrolyte [21]. For this work, electrolessly deposited samples were obtained from a commercial supplier. The details of the deposition process are proprietary; however, the Mg samples went through a pretreatment process that included alkaline cleaning, acid pickling, activation, and Zn immersion steps. Some of the coatings consisted of single Ni–P layers, while others were composed of multiple layers with Cu strike layers in some cases. Samples were chosen such that there were a range of P concentrations in the coatings, from 1.8 to 11.9 wt% (Table 1). The concentrations were measured using a scanning electron microscope (SEM) coupled with energy dispersive x-ray (EDX) spectroscopy. Figure 1 shows a schematic drawing for a multilayer coating. For all multi-layer coatings, the thickness of Ni–P above the Cu strike (t_{NiP1} in Fig. 1) was ≥ 24 µm, while the total coating thickness exceeded 30 µm for all samples. The dashed line in the t_{NiP1} layer (Fig. 1) means that the P content above or below the line may be different. For all samples in Table 1, the P content refers to the amount of P in the outermost Ni–P layer; i.e., the layer in contact with the electrolyte during testing.

2.2 Electrochemical characterization

2.2.1 Potentiodynamic polarization measurements

Potentiodynamic polarization measurements were performed using a Biologic VSP-300 potentiostat; the scan

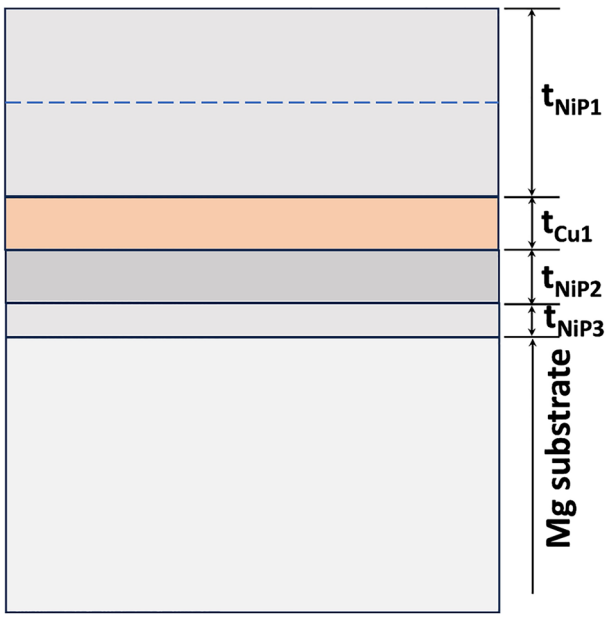

Fig. 1 Schematic drawing for coating layers. Note that not all samples have this number of layers. Specific details for coating layers for each sample are provided in Table 1

Table 1 P content and thicknesses for Ni–P coatings of all samples

Sample no.	1	2	3	4	5	6	7	8	9	10	11	12
P (wt%) outer layer	1.8	2.1	2.5	3.5	5.8	5.9	6.2	6.8	7.7	8.7	10.3	11.9
t_{NiP1} (µm) outer layer	24	24	33	24	35	35	30	25	41	24	33	33
t_{Cu1} (µm)	7	7	–	5	–	–	–	7	8	7	–	–
t_{NiP2} (µm)	–	–	2–3	7	2–3	2–3	–	11	2–3	2–3	2–3	2–3
t_{NiP3} (µm)	–	–	–	2–3	–	–	–	2–3	–	–	–	–
Total thickness (µm)	31	31	35	40	38	38	30	45	50	35	35	35

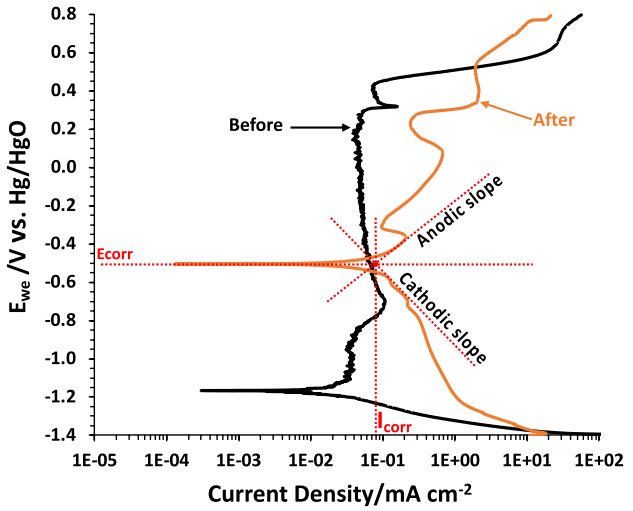

Fig. 2 Potentiodynamic polarization curves before and after cycle testing for Sample 11

speed was set at 1 mV/s with a potential range of − 0.8 to 0.4 V. A Hg/HgO reference electrode was employed along with a graphite counter electrode. The corrosion potential E_{corr} and corrosion current density I_{corr} were determined from measured Tafel plots using EC-Lab software, within the potential range of ± 100 mV by finding the intersection of the anodic slope and cathodic slope (Fig. 2). The area exposed to the corrosive medium (11 M KOH, 125 mL) was ~ 1 cm^2, with non-exposed portions covered with epoxy. All electrochemical measurements were carried out at room temperature (21 °C), without degassing the electrolyte.

2.2.2 Cycle testing

Galvanostatic cycling potential limitation (GCPL) tests for the Ni–P coatings were carried out to simulate the HER and OER processes in a zinc-air flow battery (ZAFB) cell with 11 M KOH electrolyte at room temperature without degassing the electrolyte before testing. Measurements were done by periodically applying constant negative and positive currents with a short rest period when switching the current from negative to positive or vice versa, while recording the discharge and charge voltage response. The experimental settings were the same as those in Sect. 2.2.1. The cycling test parameters are listed in Table 2, where E_{we} is the working electrode voltage. All cycling tests were carried out at room temperature and most samples were tested for 2000 cycles (the minimum desired lifetime). One sample (Sample 9) was also tested for 10,000 cycles to measure any possible corrosion rate changes with extended cycling.

Table 2 Experimental conditions for galvanostatic cycling potential limitation (GCPL) test

Step	Step description
Open circuit potential (OCV)	10 s
HER	− 100 mA cm^{-2} for 25 s; $E_{we} \geq -1.8$ V vs. Hg/HgO
OCV	10 s
OER	+ 100 mA cm^{-2} for 40 s; $E_{we} \leq 1.5$ V vs. Hg/HgO

2.3 Pore density and pore areal fraction determination

Pore sizes in the Ni–P coatings were measured from SEM back scattered electron (BSE) images of polished cross section samples. Pore shapes were irregular, so to be consistent pore sizes were measured as the largest diameters and pore areal fractions were estimated based on the assumption that the pores were circular. Pore numbers and diameters were measured using ImageJ software and then converted to pore areal densities and pore areal fractions.

2.4 Scanning electron microscopy (SEM)

All samples were examined in cross section orientation, before and after electrochemical testing, using scanning electron microscopy (Tescan Vega3 SEM or Zeiss Sigma VP 300-FESEM). The samples were cold mounted, followed by mechanical grinding, and then final polishing using a 0.05 µm Al_2O_3 suspension. The polished samples were coated with a thin layer of evaporated carbon prior to SEM examination. Ni–P coating thicknesses were measured from BSE images before and after electrochemical cycling from the same samples. BSE images provided atomic number contrast and allowed the various coating layers to be easily identified. Composition analysis of the various layers was done using energy dispersive x-ray (EDX) microanalysis (X-MaxN 20, Oxford Instruments, or Bruker dual silicon drift detectors). BSE imaging analysis for all samples were done at the same accelerating potential (20 kV), the same working distance (14 mm), and the same magnifications. For each sample, five BSE images

were obtained and coating thicknesses were measured at five locations per image, giving a total of 25 measured thicknesses for each sample.

3 Results and discussion

For corrosion testing in neutral electrolytes (e.g., 3.5 wt% NaCl) or mildly acidic electrolytes (water diluted HCl or H_2SO_4), there is a consensus in the literature that the corrosion current I_{corr} decreases as the P concentration in Ni–P increases [5–8, 22–25]. However, the situation for alkaline solutions is different, as mentioned above, based on polarization and electrochemical impedance spectroscopy (EIS) experiments Lo et al. [12], Kang et al. [13], and Zeller et al. [14] obtained different corrosion resistance.

The various Ni–P coatings were cycle tested. Potentiodynamic polarization curves (i.e., Tafel plots) were obtained before and after cycle testing; examples for coating 11 are shown in Fig. 2. E_{corr} and I_{corr} values were extracted from the plots (Table 3) and I_{corr} values were converted to corrosion rates (CR) based on Faraday's Law using Eq. (1) [26] and plotted as a function of P content in the outer Ni–P layer (Fig. 3).

$$\mathrm{CR} = K_1 \frac{I_{corr}}{\rho} \mathrm{EW}, \tag{1}$$

where CR is given in nm h^{-1} and I_{corr} in μA cm^{-2}. K_1 is equal to 0.373 nm g (μA cm h)$^{-1}$, ρ is the density of the corroding metal (8.908 g cm^{-3} for pure Ni was assumed), and EW is the dimensionless equivalent weight, which is given as W/n (W is the atomic weight of the element and n is the valence

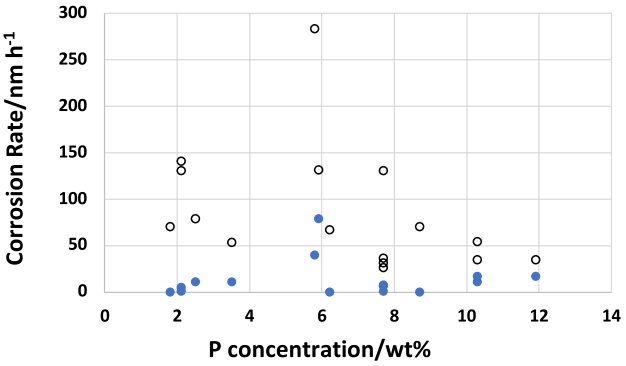

Fig. 3 Relationship between calculated corrosion rates (CR) from I_{corr} and P concentration for electroless Ni–P coatings. The dots represent corrosion rates before cycle testing, while the open circles represent corrosion rates after cycle testing

for the corroding metal, which is 2 for Ni). In all cases, there is an increase in corrosion rate for the post-cycled samples compared with the pre-cycled samples. In addition, although there is considerable scatter, the corrosion rate is highest at intermediate P compositions (~6 wt%) and reduced at lower and higher P concentrations.

The use of I_{corr} to determine corrosion rate is an indirect method. A direct approach was taken by measuring the layer thicknesses of regions that were not exposed to the electrolyte and regions that were exposed to the electrolyte. The average corrosion rate is then just the difference in coating thickness divided by the cycle testing time. Examples of SEM BSE cross section images for non-cycled and cycled regions are shown in Fig. 4. It is clear that corrosion of the Ni–P coating is not localized, but occurs uniformly across the sample. The example in Fig. 4a corresponds to Sample

Table 3 E_{corr} and I_{corr} before GCPL and after GCPL testing, as well as corresponding corrosion rates (CR)

Sample	P (wt%)	Before GCPL E_{corr} (mV)	After GCPL E_{corr} (mV)	Before GCPL I_{corr} (μA cm^{-2})	CR before GCPL (nm h^{-1})	After GCPL I_{corr} (μA cm^{-2})	CR after GCPL (nm h^{-1})
1	1.8	− 504.5	334.7	0.05	0.1	56.7	69.7
2	2.1	− 161.7	489.4	3.61	4.4	105.8	130.2
3	2.5	− 728.4	− 731.5	8.96	11.0	63.6	78.2
4	3.5	− 755.6	− 539.2	8.48	10.4	43.2	53.2
5	5.8	231.3	475.1	32.47	39.9	230.3	283.2
6	5.9	240.8	435.4	63.63	78.2	106.7	131.2
7	6.2	− 527.3	353.5	0.01	0.0	54.2	66.8
8	6.8	197.3	359.8	0.44	0.5	21.2	26.1
9	7.7	− 1160.0	− 758.7	5.64	6.9	25.6	31.4
9	7.7	− 736.0	− 543.6	3.87	4.8	79.4	97.7
10	8.7	− 285.6	306.4	0.13	0.2	95.5	117.4
11	10.3	− 768.7	− 493.1	8.58	10.6	43.9	54.0
12	11.9	− 1169.0	− 503.2	13.44	16.5	28.0	34.4

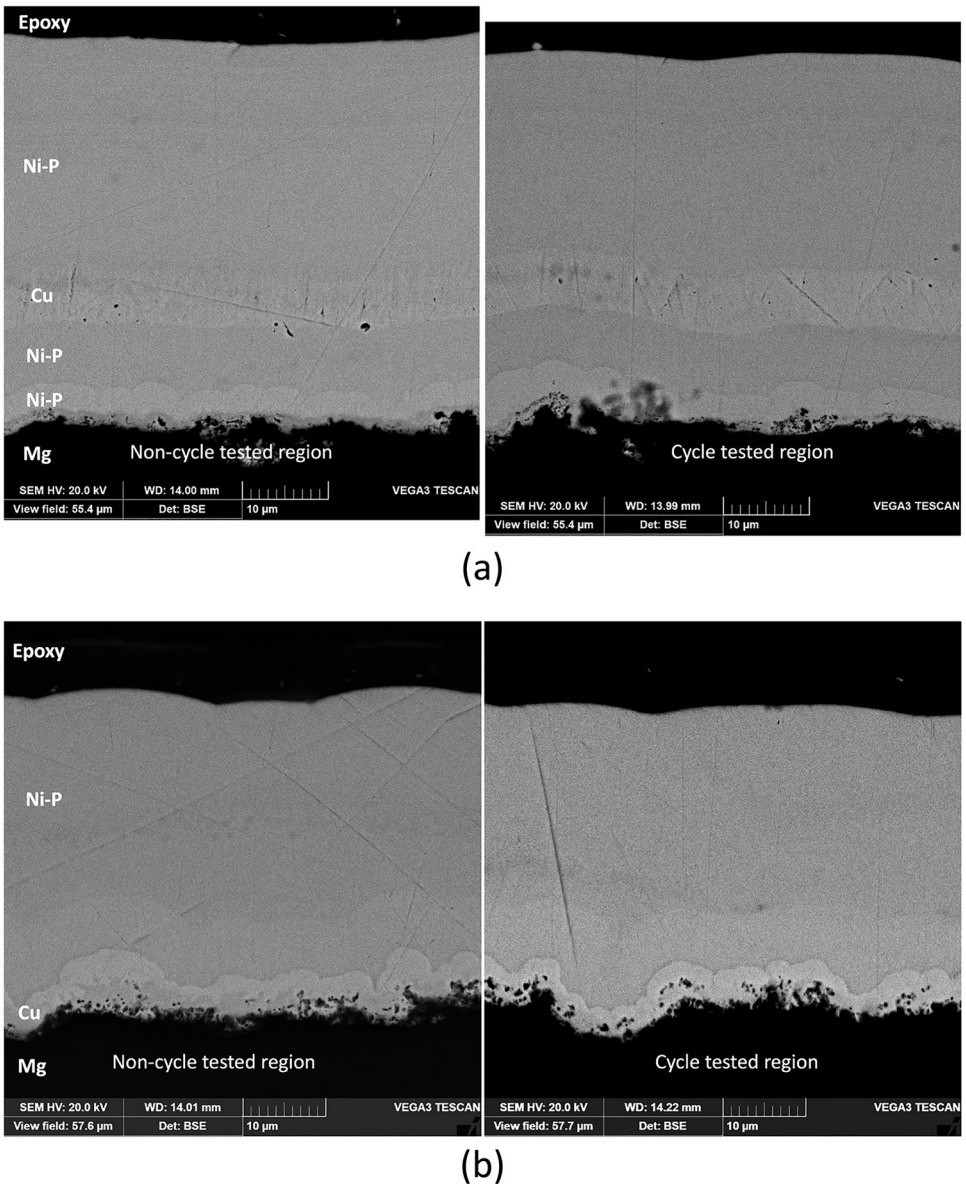

Fig. 4 **a** SEM BSE images of Sample 8 showing coating thicknesses from non-cycle tested (left) and cycle tested (right) regions. **b** SEM BSE images of Sample 11 showing coating thicknesses from non-cycle tested (left) and cycle tested (right) regions

8 and represents a case where corrosion of the outer Ni–P layer is clearly apparent. The example in Fig. 4b indicates a case (Sample 11) where the amount of corrosion is low. For many of the samples, the Cu strike layer was utilized as a marker layer for the coating thickness measurements.

The thickness changes and corresponding average corrosion rates are provided in Table 4. The average corrosion rate as a function of P content in the outermost Ni–P layer is plotted in Fig. 5. The behavior is not linear, but exhibits a parabolic shape. The corrosion rates are lowest at the highest and lowest P compositions, with the highest rates at intermediate compositions in the 6–8 wt% P range. This behavior is similar qualitatively, but more obvious, to that shown in Fig. 3, where corrosion rates extracted from I_{corr} values were plotted against P composition. To the authors' knowledge, this is the first time that corrosion rate has been correlated with the P contents in Ni–P coatings through direct measurements of coating thickness changes under the same corrosion conditions, rather than just indirectly from corrosion currents. Although the results are qualitatively similar for both indirect (polarization curves) and direct measurements, the indirect measurements can, in some instances, provide corrosion rates significantly in excess of actual values (e.g., Samples 5, 6 and 10—Tables 3 and 4). Inconsistencies can arise in the way that I_{corr} values are obtained from polarization curves, due to the nature of the curves and because current densities are plotted on a log scale. The work by Zeller and Salvati [14], for Ni–P coatings in NaOH electrolyte, reported an opposite corrosion dependence with P content. The lowest corrosion rate was observed for intermediate P levels (e.g., 5.0 wt% P), although their rates were determined indirectly; i.e., through electrochemical measurements such

Table 4 Thickness change for samples after cycle testing measured by SEM

Sample	P (wt%)	Cycles	Thickness change (nm)	Corrosion rate (nm h^{-1})
1	1.8	2000	2006	42.5
2	2.1	2000	1751	37.1
3	2.5	2000	1795	38.0
4	3.5	2000	1996	42.3
5	5.8	2000	2324	49.2
6	5.9	2000	2455	52.0
7	6.2	2000	2421	51.3
8	6.8	2000	2277	48.2
9	7.7	2000	2079	44.0
9	7.7	10,000	11,645	49.3
10	8.7	3359	4170	52.3
11	10.3	2000	1820	38.6
12	11.9	2000	1626	34.4

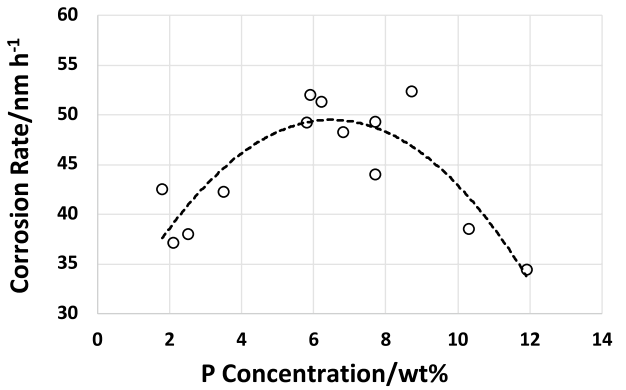

Fig. 5 Relationship between corrosion rate and P content in the outermost Ni–P layer of the coatings

as polarization electrochemical impedance spectroscopy. In addition, their electrolyte (NaOH) was different than that used in this work.

Cycle testing was also done for 10,000 cycles for Sample 9 using the same set of parameters; the results are shown in Fig. 6. Figure 6a is from the unexposed region (no cycling), Fig. 6b is from the region tested for 2000 cycles, and Fig. 6c is from the region that underwent 10,000 cycles. The average thickness change after 2000 cycles is 2079 nm, while the average thickness change is 11,645 nm after 10,000 cycles. These values correspond to average corrosion rates of 44.0 nm h^{-1} and 49.3 nm h^{-1}, respectively, which indicate that the corrosion process does not vary significantly with time.

It is interesting to note that the parabolic shape of CR vs P content curve is very similar to that for coating stress vs P content reported by Duncan in 1996 [27] and shown in Fig. 7. In Fig. 7, the dots, showing stress vs P content, were reproduced from Fig. 3 of Duncan's work [27]. The dotted line has been added by the current authors to better illustrate the trend for the distribution of stress vs P content. To compare the stress distribution vs P content with the corrosion rate distribution vs P content, Fig. 5 is superimposed on Fig. 7 (shown as open circles and dashed curve). As pointed out by Duncan, at P concentrations below ~ 4 wt% or above ~ 11 wt% the internal stress within the coatings is compressive, while coatings with compositions between these values exhibit tensile stresses. The corrosion rate vs P distribution essentially follows Duncan's distribution of stress vs P content.

As discussed at the beginning of this section, the corrosion resistance of Ni–P coatings increases with increasing P content in neutral and acidic solutions. This is quite different from the behavior in the present work for alkaline solutions, which suggests that the corrosion mechanism for Ni–P coatings in neutral/acidic solutions is different from that in alkaline solutions. Based on XPS measurements, Diegle et al. [28] proposed that, for acidic and neutral solutions, a layer of phosphite anions can be generated on the Ni–P coating surface, forming a barrier layer between the coating and the electrolyte. This layer can block water access to the coating surface, thereby inhibiting hydration of nickel. It is likely that a higher P coating has a greater probability to form this barrier layer, enhancing the chances of blocking hydration of the Ni–P coating. As such, one would expect coatings with higher P levels to have better corrosion resistance. For alkaline solutions, the phosphite layer does not form on the surface; however, both Kang et al. [13] and Zeller et al. [14] showed through XPS measurements that the P content is depleted in the near surface region of the coating, which indicates that P at the alloy surface is consumed upon sample exposure to the electrolyte. As such, the Ni–P coating can directly contact the electrolyte, forming a layer of $Ni(OH)_2$ on the coating surface. In this scenario, the type of stress within the coating becomes important in terms of the corrosion resistance.

Generally, tensile stresses are not favorable in terms of corrosion resistance [29–31], since tensile loads may open cracks or weaken coating coverage and may also accelerate metallic ion dissolution into the electrolyte, or water diffusion into the Ni–P coating. On the other hand, compressive stresses in coatings can inhibit crack initiation or crack growth, thereby reducing corrosion rates. If coating stress is unavoidable, then compressive stresses are preferred relative to tensile stresses. As such, coatings with P levels either below 3.5 wt% or above 11 wt% are favorable for Ni–P coatings utilized in 11 M KOH electrolytes.

The thickness of the phosphite layer or $Ni(OH)_2$ layer on the coating surface is likely less than 10 nm, since for all Ni 2p peak spectra presented in [13, 14], the Ni° peaks

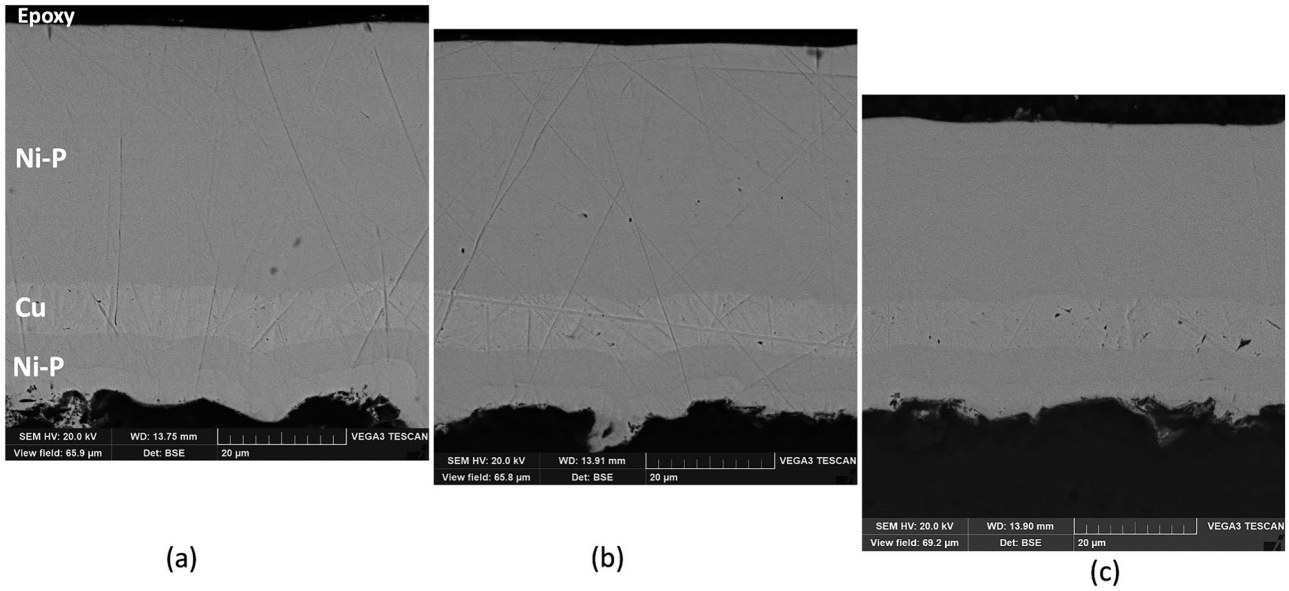

Fig. 6 SEM BSE images from sample 9: **a** non-cycle tested region, **b** 2000 cycles, and **c** 10,000 cycles

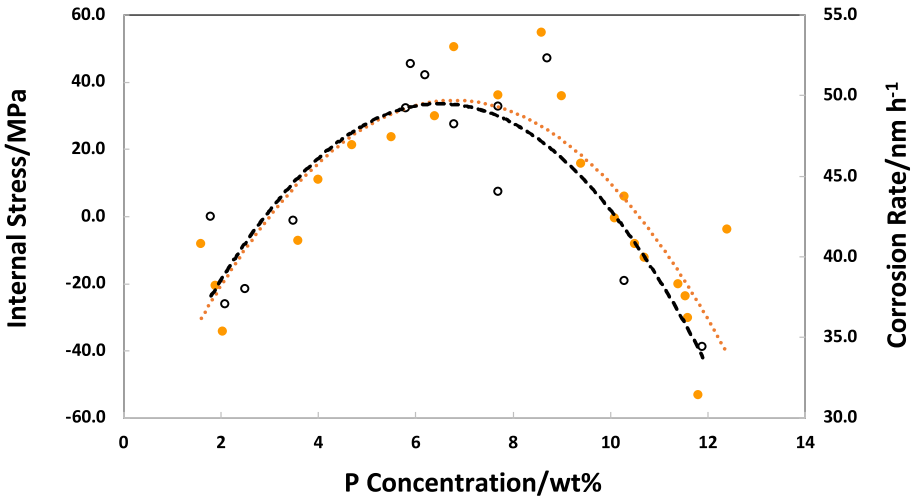

Fig. 7 Relationship between internal stress and P concentration in Ni–P coatings (dot symbols), reproduced from Duncan's work [27]. The dotted curve has been added by the authors to show the data trend. The present work showing the relationship between corrosion rate and P content has been superimposed (black open circle symbols and black dashed curve) on Duncan's results

are strong. The layer (either the phosphite layer or $Ni(OH)_2$ layer) on the Ni–P surface does not attenuate the Ni° signal very much. The depth resolution for XPS technique is typically less than 10 nm [32], so that the appearance of strong Ni° peaks means that surface phosphite or $Ni(OH)_2$ layer is very thin. In fact, a surface layer was not detected during FESEM imaging.

It should be noted that the corrosion rates shown in Fig. 5 were obtained under the cycling test conditions listed in Table 2. Changing the cycling test parameters for the coatings, such as different current densities and durations, will affect the corrosion rates for the coatings. However, the relationship between corrosion rate and P concentration follows the dependence shown in Fig. 5.

For comparison purposes, cross section analysis was also done for a sample immersed in 11 M KOH for 49 days without any applied current. There was no measurable change in coating thickness before and after immersion. As such, the corrosion of Ni–P coatings under immersion conditions only is minimal, which is consistent with Zeller et al.'s report for immersion testing of Ni–P coatings in 50% NaOH electrolyte [14].

To confirm that the corrosion rates of Ni–P coatings are indeed dependent on P content and not other factors, such as coating porosity, pore fraction and areal density were measured from SEM cross section images. The effect of porosity on Ni–P coating corrosion behavior in alkaline solutions has not been reported previously. The results,

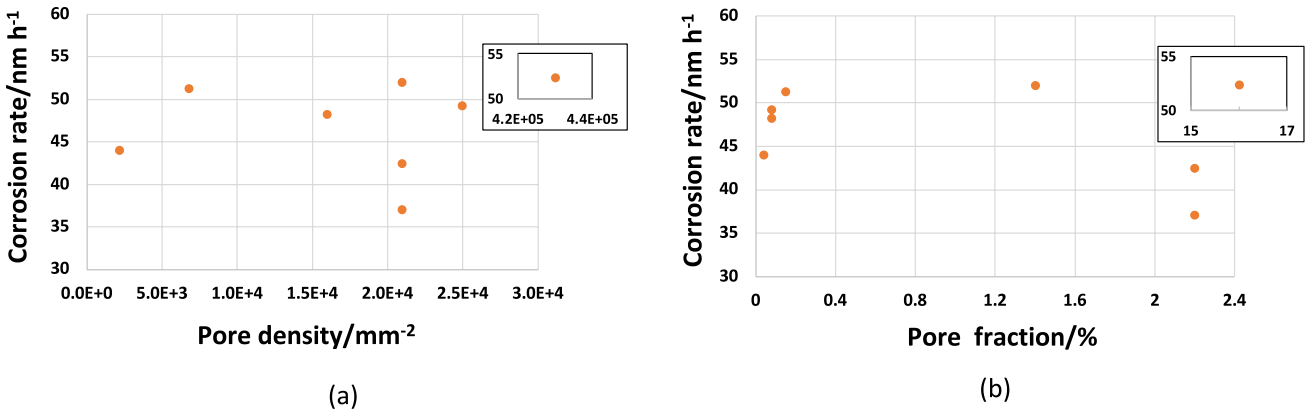

Fig. 8 Relationship between **a** corrosion rate and pore density and **b** corrosion rate and pore area fraction for Samples 1, 2, 5, 6, 7, 9, 10 and 12. Pore sizes were below 4 µm in diameter, with most smaller than 2 µm. The insets show results from Sample 10, which had significantly higher pore density and pore fraction. There is no obvious relationship between corrosion rate and pore density/pore fraction

for 8 of the coatings, are presented in Fig. 8 and reveal no clear relationship between corrosion rate and pore density or pore fraction. One could argue that there is a weak trend indicating that corrosion rate decreases slightly as pore fraction increases. This behavior seems counterintuitive, as increased porosity would presumably lead to increased corrosion [33–35]. The pores for the Ni–P coatings in this work are likely isolated in nature; i.e., do not continuously propagate from the substrate/coating interface to the coating surface. As such, porosity does not enhance corrosion rates. To confirm the nature of the porosity, several solutions were analyzed using atomic absorption spectroscopy (AAS), before and after cycling testing. In all cases, Mg levels in the electrolyte were below the detectability limit of AAS (0.07 ppm Mg), indicating that no Mg dissolution occurred. Mg dissolution would require extension of pores from the coating surface to the Mg/coating interface.

4 Conclusions

The corrosion behavior of 12 Ni–P coatings, electrolessly deposited on Mg substrates in highly alkaline KOH (11 M) electrolytes, was investigated using cyclic testing where samples were exposed to oxygen evolution reaction and hydrogen evolution reaction conditions. Corrosion rates were determined both indirectly through I_{corr} measurements from polarization curves and directly through SEM measurements of cross section samples. Corrosion rates were found to correlate with the P content in the Ni–P coatings, which appeared to correspond to stress levels in the coatings. Corrosion rates were lowest for P concentrations below ~ 3.5 wt% and above ~ 11 wt%, which correlates with compressive stresses within the coatings. The corrosion rate trends determined from direct and indirect measurements are similar; however, indirect measurements are more variable and, as such, direct measurements are recommended whenever possible to obtain more reliable corrosion rates.

Acknowledgements The authors are grateful to the Natural Sciences and Engineering Research Council of Canada (NSERC – Grant #ALLRP 566309-2021), the University of Alberta Future Energy Systems (FES T06 P03) and Zinc8 Energy Solutions for funding support. Zinc8 is also acknowledged for providing coating samples.

Author contributions A.H. wrote the main manuscript text, prepared most of the tables and figures, and performed the microscopy analysis. H.H. performed the electrochemical testing, prepared Fig. 2 and Tables 2 and 3, and contributed to data analysis. D.A. provided the samples and contributed to experimental design and data interpretation. D.I. supervised the project and contributed to experimental design, data interpretation, and writing of the manuscript. All authors reviewed the manuscript.

Data availability Data is provided within the manuscript.

Declarations

Competing interests The authors declare no competing interests.

References

1. Chintada VB, Koona R, Bahubalendruni MVAR (2021) State of art review on nickel-based electroless coatings and materials. J Bio Tribo-Corros 7:134. https://doi.org/10.1007/s40735-021-00568-7
2. Nazari H, Darband GB, Arefinia R (2023) A review on electroless Ni–P nanocomposite coatings: effect of hard, soft, and synergistic nanoparticles. J Mater Sci 58:4292–4358. https://doi.org/10.1007/s10853-023-08281-1
3. Muraliraja R, Selvan RAS, Selvakumar A, Franco M, Tamilarasan TR, Sanjith U, Sha W, Sudagar J (2023) A review of electroless coatings on non-metals: bath conditions, properties, and applications. J Alloys Compd 960:170723. https://doi.org/10.1016/j.jallcom.2023.170723

4. Shozib IA, Ahmad A, Abdul-Rani AM, Beheshti M, Aliyu AA (2022) A review on the corrosion resistance of electroless Ni-P based composite coatings and electrochemical corrosion testing methods. Corros Rev 40:1–37. https://doi.org/10.1515/corrrev-2020-0091
5. Fayyad EM, Abdullah AM, Hassan MK, Mohamed AM, Jarjoura G, Farhat Z (2018) Recent advances in electroless-plated Ni-P and its composites for erosion and corrosion applications: a review. Emerg Mater 1:3–24. https://doi.org/10.1007/s42247-018-0010-4
6. Gu C, Lian J, He J, Jiang Z, Jiang Q (2006) High corrosion-resistance nanocrystalline Ni coating on AZ91D magnesium alloy. Surf Coat Technol 200:5413–5418. https://doi.org/10.1016/j.surfcoat.2005.07.001
7. Zuleta AA, Galvis OA, Castano JG, Echeverria F, Bolivar FJ, Hierro MP, Perez-Trujillo FJ (2009) Preparation and characterization of electroless Ni–P–Fe_3O_4 composite coatings and evaluation of its high temperature oxidation behavior. Surf Coat Technol 203:3569–3578. https://doi.org/10.1016/j.surfcoat.2009.05.025
8. Wang Y, Liu H, Bi S, He M, Wang C, Cao L (2016) Effects of organic additives on the immersion gold depositing from a sulfite–thiosulfate solution in an electroless nickel immersion gold process. RSC Adv 6:9656–9662. https://doi.org/10.1039/C5RA17975K
9. Elsener B, Crobu M, Scorciapino MA, Rossi A (2008) Electroless deposited Ni–P alloys: corrosion resistance mechanism. J Appl Electrochem 38:1053–1060. https://doi.org/10.1007/s10800-008-9573-8
10. Ashassi-Sorkhabi H, Aminikia H, Bagheri R (2014) Electroless deposition of Ni-Cu-P coatings containing nano-Al_2O_3 particles and study of its corrosion protective behavior in 0.5 M H_2SO_4. Int J Corros 2014:391502. https://doi.org/10.1155/2014/391502
11. Li L, Wang J, Xiao J, Yan J, Fan H, Sun L, Xue L, Tang Z (2021) Time-dependent corrosion behavior of electroless NieP coating in H_2S/Cl-environment. Int J Hydrogen Energy 46:11849–11864. https://doi.org/10.1016/j.ijhydene.2021.01.053
12. Lo PH, Tsai WT, Lee JT, Hung MP (1995) The electrochemical behavior of electroless plated Ni-P alloys in concentrated NaOH solution. J Electrochem Soc 142:91–96. https://doi.org/10.1149/1.2043954
13. Kang J, Yang Y, Shao H (2009) Comparing the anodic reactions of Ni and Ni–P amorphous alloy in alkaline solution. Corros Sci 51:1907–19013. https://doi.org/10.1016/j.corsci.2009.04.032
14. Zeller RL III, Salvati L Jr (1994) Effects of phosphorus on corrosion resistance of electroless nickel in 50% sodium hydroxide. Corrosion 50(6):457–467. https://doi.org/10.5006/1.3293524
15. Madrama AR, Pourfarzad H, Zare HR (2012) Study of the corrosion behavior of electrodeposited Ni–P and Ni–P–C nanocomposite coatings in 1 M NaOH. Electrochim Acta 85:263–326. https://doi.org/10.1016/j.electacta.2012.08.061
16. Shervedani RK, Alinoori AH, Madram AR (2008) Electrocatalytic activities of nickel-phosphorous composite coating ceinforced with codeposited graphite carbon for hydrogen evolution reaction in alkaline solution. J New Mater Electrochem Syst 11:259–265
17. Smedley SI, Zhang XG (2007) A regenerative zinc–air fuel cell. J Power Sources 165:897–904. https://doi.org/10.1016/j.jpowsour.2006.11.076
18. Paul MTY, Yee BB, Bruce DR, Gates BD (2017) Hexagonal arrays of cylindrical nickel microstructures for improved oxygen evolution reaction. ACS Appl Mater Interfaces 9(8):7036–7043. https://doi.org/10.1021/acsami.6b14129
19. Khor A, Leung P, Mohamed MR, Flox C, Xu Q, An L, Will RGA, Morante JR, Shah AA (2018) Review of zinc-based hybrid flow batteries: from fundamentals to applications. Mater Today Energy 8:80–108. https://doi.org/10.1016/j.mtener.2017.12.012
20. Petro R, Schlesinger M (2012) Direct electroless deposition of low phosphorus Ni-P films on AZ91D Mg alloy. J Electrochem Soc 159(7):D455–D461. https://doi.org/10.1149/2.069207jes
21. Małecki A, Micek-Ilnicka A (2000) Electroless nickel plating from acid bath. Surf Coat Technol 123:72–77. https://doi.org/10.1016/S0257-8972(99)00423-5
22. Balaraju JN, Selvi VE, Grips VKW, Rajam KS (2006) Electrochemical studies on electroless ternary and quaternary Ni–P based alloys. Electrochim Acta 52:1064–1074. https://doi.org/10.1016/j.electacta.2006.07.001
23. Li N, Cui G, Li D, Zheng J, Wu Q (2006) The physical and electrochemical properties of electroless deposited nickel–phosphorus black coatings. Surf Coat Technol 200:6808–6814. https://doi.org/10.1016/j.surfcoat.2005.10.015
24. Sankara Narayanan TSN, Baskaran I, Krishnaveni K, Parthiban S (2006) Deposition of electroless Ni–P graded coatings and evaluation of their corrosion resistance. Surf Coat Technol 200:3438–3445. https://doi.org/10.1016/j.surfcoat.2004.10.014
25. Shibli SMA, Dilimon VS (2007) Effect of phosphorous content and TiO_2-reinforcement on Ni–P electroless plates for hydrogen evolution reaction. Int J Hydrogen Energy 32:1694–1700. https://doi.org/10.1016/j.ijhydene.2006.11.037
26. ASTM G102-89 (1994) Standard practice for calculation of corrosion rates and related information from electrochemical measurements. Annual book of ASTM standards, vol 03.02
27. Duncan RN (1996) The metallurgical structure of electroless nickel deposits: effect on coating properties. Plat Surf Finish 8:65–69
28. Diegle RB, Sorensen NR, Clayton CR, Helfand MA, Yu YC (1988) An XPS investigation into the passivity of an amorphous Ni-20P alloy. J Electrochem Soc 135:1085–1092
29. Song YW, Shan DY, Han EH (2008) High corrosion resistance of electroless composite plating coatings on AZ91D magnesium alloy. Electrochim Acta 53:2135–2143. https://doi.org/10.1016/j.electacta.2007.09.026
30. Alanzi NM, EL-Sherik AM, Alamar SH, Shen S (2013) Influence of residual stresses on corrosion and wear behavior of electrodeposited nanocrystalline cobalt-phosphorus coatings. Int J Electrochem Sci 8:10350–10358. https://doi.org/10.1016/S1452-3981(23)13115-4
31. Liu H, Qian DS (2018) Evaluation of residual stress and corrosion behavior of electroless plated Ni−P/Ni−Mo−P coatings. Trans Nonferrous Met Soc China 28:2499–2510. https://doi.org/10.1016/S1003-6326(18)64896-4
32. Stevie FA, Donley CL (2020) Introduction to x-ray photoelectron spectroscopy. J Vac Sci Technol A 38:063204. https://doi.org/10.1116/6.0000412
33. Zhang WX, Jiang ZH, Li GY, Jiang Q, Lian JS (2008) Electroless Ni-Sn-P coating on AZ91D magnesium alloy and its corrosion resistance. Surf Coat Technol 202:2570–2576. https://doi.org/10.1016/j.surfcoat.2007.09.023
34. Lian JS, Li GY, Niu LY, Gu CD, Jiang ZH, Jiang Q (2006) Electroless Ni-P deposition plus zinc phosphate coating on AZ91D magnesium alloy. Surf Coat Technol 200:5956–5962. https://doi.org/10.1016/j.surfcoat.2005.09.007
35. Li J, Tian Y, Huang Z, Zhang X (2006) Studies of the porosity in electroless nickel deposits on magnesium alloy. Appl Surf Sci 252:2839–2846. https://doi.org/10.1016/j.apsusc.2005.04.028